AMERICAN SOCIETY FOR MICROBIOLOGY | Infection and Immunity®

MOLECULAR PATHOGENESIS

The Integrative Conjugative Element ICESpyM92 Contributes to Pathogenicity of Emergent Antimicrobial-Resistant *emm92* Group A *Streptococcus*

Luis Alberto Vega,[a] Misu A. Sanson,[a] María Belén Cubria,[a] Shrijana Regmi,[a] Brittany J. Shah,[a] Samuel A. Shelburne,[c] Anthony R. Flores[a,b]

[a]Division of Infectious Diseases, Department of Pediatrics, McGovern Medical School, University of Texas Health Sciences Center at Houston, Houston, Texas, USA
[b]Center for Antimicrobial Resistance and Microbial Genomics, University of Texas Health Sciences Center at Houston, Houston, Texas, USA
[c]Department of Infectious Diseases, Division of Internal Medicine, The University of Texas MD Anderson Cancer Center, Houston, Texas, USA

ABSTRACT Antimicrobial resistance-encoding mobile genetic elements (MGEs) may contribute to the disease potential of bacterial pathogens. We previously described the association of Group A *Streptococcus* (GAS) derived from invasive disease with increasingly frequent antimicrobial resistance (AMR). We hypothesized that a 65-kb AMR-encoding MGE (ICESpyM92), highly conserved among closely related emergent invasive *emm92* GAS, contributes to GAS disease potential. Here, we provide evidence that a combination of ICESpyM92- and core genome-dependent differential gene expression (DGE) contributes to invasive disease phenotypes of emergent *emm92* GAS. Using isogenic ICESpyM92 mutants generated in distinct *emm92* genomic backgrounds, we determined the presence of ICESpyM92 enhances GAS virulence in a mouse subcutaneous infection model. Measurement of *in vitro* and *ex vivo* DGE indicates ICESpyM92 influences GAS global gene expression in a background-dependent manner. Our study links virulence and AMR on a unique MGE via MGE-related DGE and highlights the importance of investigating associations between AMR-encoding MGEs and pathogenicity.

KEYWORDS *Streptococcus pyogenes*, antimicrobial resistance, virulence, mobile genetic element, transcriptome

Antimicrobial resistance (AMR) in bacterial pathogens is an alarming threat to human health. Mobile genetic elements (MGEs), such as plasmids, transposons, and integrative conjugative elements (ICEs), are a major source of AMR genes. AMR-encoding MGEs are widespread in the absence of antimicrobial pressure, raising the possibility that additional factors are involved in their maintenance and dissemination. Data suggest that AMR-encoding MGEs may contribute to bacterial virulence in a variety of ways. MGEs can encode virulence genes alongside AMR elements, like the phenol-soluble modulin in the SCCmec element of methicillin-resistant *Staphylococcus aureus* (1). MGEs may also encode virulence proteins that alter antimicrobial susceptibility, such as the YbtPQ siderophore importer in *Klebsiella pneumoniae* (2). MGE gene content can even indirectly influence virulence, as does an sRNA associated with the aminoglycoside resistance locus of a plasmid-borne integron in *Acinetobacter baumannii* (3). Therefore, the association of AMR with factors contributing to virulence on MGEs that can be horizontally transferred between bacterial strains and species requires investigation if the emergence of AMR is to be effectively countered.

Streptococcus pyogenes (Group A *Streptococcus*, GAS) is an exclusively human pathogen that primarily colonizes the epithelia of the human throat and skin. GAS serotypes that have emerged over the past 30 years (e.g., *emm1*, *emm3*, *emm89*, and *emm28*) are

Editor Nancy E. Freitag, University of Illinois at Chicago

Address correspondence to Anthony R. Flores, anthony.r.flores@uth.tmc.edu.
The authors declare no conflict of interest.
Received 18 February 2022
Returned for modification 31 March 2022
Accepted 9 July 2022
Published 1 August 2022

responsible for an upsurge in invasive disease associated with high mortality rates (4). Acquisition of MGEs in GAS contributes to enhanced virulence, clone emergence, and niche specialization. Prophage-encoded virulence factors, such as pyrogenic exotoxins (SpeA and SpeK), phospholipases (Sla) or DNAses (Sdn and Sda), contribute to the disease potential of *emm1* and *emm3* GAS (5–7). The MGE dubbed Region of Difference 2 (RD2) has been associated with *emm28* strain prevalence in puerperal sepsis cases (8). Horizontal transfer of RD2 into other strain backgrounds enhanced GAS colonization of murine vaginal infection models (9), further suggesting MGE acquisition potentially contributes to GAS disease phenotypes.

GAS remains universally susceptible to β-lactams and thus have not, historically, been the focus of AMR research. However, recent epidemiological data reveal increasingly frequent GAS invasive disease in the United States attributable to macrolide-resistant strains (10), particularly among persons experiencing homelessness and/or intravenous drug use (11). Most invasive AMR GAS infections in the United States from 2006 to 2017 were due to a subset of *emm* types (*emm11*, *58*, *77*, *83*, and *92*), with *emm92* contributing the largest increase in erythromycin-nonsusceptibility (10). Whole genome sequencing analysis of *emm11*, *75*, *77*, and *emm92* invasive AMR strains revealed that diverse MGEs encode AMR in GAS, including ICEs, prophages, and plasmids (12). The presence of similar invasive AMR GAS among pediatric (12) and at-risk populations (e.g., adults experiencing homelessness and/or intravenous drug use) (11, 13) indicates a concerning dissemination of resistance.

We recently described tetracycline and aminoglycoside resistance encoded in a highly conserved 65-kb ICE (ICESpyM92) among *emm92* GAS strains nearly exclusively isolated from invasive or skin and soft tissue infections (SSTIs) over the span of several years (2015–2017) across multiple surveillance sites in the United States (12). We hypothesized that ICESpyM92 gene content contributes to GAS disease potential. Our investigation of isogenic ICESpyM92 mutants indicates that a combination of ICESpyM92-dependent and independent gene transcription influences *emm92* virulence. Our findings show that an AMR-encoding ICE can promote bacterial virulence, thereby providing potential insights into maintenance and dissemination of such elements in the population even in the absence of antimicrobial pressure.

RESULTS

Emergent *emm92* GAS exhibits enhanced virulence in a murine model of SSTI. Our previous study revealed that contemporary AMR *emm92* (henceforth referred to as emergent *emm92*) constitutes a highly clonal population in which ICESpyM92 is well conserved, suggesting recent emergence (12). We hypothesized that emergence of AMR *emm92* may be, at least in part, due to increased virulence associated with ICESpyM92. To test this hypothesis, we first investigated whether emergent *emm92* virulence differs from that of the antimicrobial susceptible invasive *emm92*, MGAS270 (14). MGAS270 was isolated in the late 1980s from a patient with severe invasive disease. Using whole genome sequencing (WGS) and antimicrobial susceptibility testing (data not shown), we confirmed MGAS270 lacks AMR-encoding elements, including ICESpyM92 and the erythromycin resistance-encoding pRW35-like plasmid (Fig. 1). While MGAS270 differs from the contemporary reference strain, TSPY556, by 115 single nucleotide polymorphisms (Fig. 1), in the absence of readily available, more closely related, ICESpyM92-negative contemporary *emm92* GAS strains, MGAS270 was used to represent the ICESpyM29-negative *emm92* population. We compared emergent *emm92* and MGAS270 virulence by measuring GAS colonization burden and necrotic lesion development in a mouse SSTI model (15, 16). Mice were infected subcutaneously in one flank with an emergent *emm92* strain (TSPY1285) (12) and in the other flank with MGAS270 (Fig. 2A). The median necrotic lesion size 48 hours postinfection (hpi) was significantly greater at sites infected with emergent *emm92* (Fig. 2B; $P = 0.0064$), as well as at multiple time points in the course of the 7-day monitoring period (Fig. 2C; $P < 0.05$). Harvesting of infected tissue for enumeration of bacterial burden revealed well-defined abscesses predominantly formed at MGAS270 (ICE[–]) infection sites, whereas more

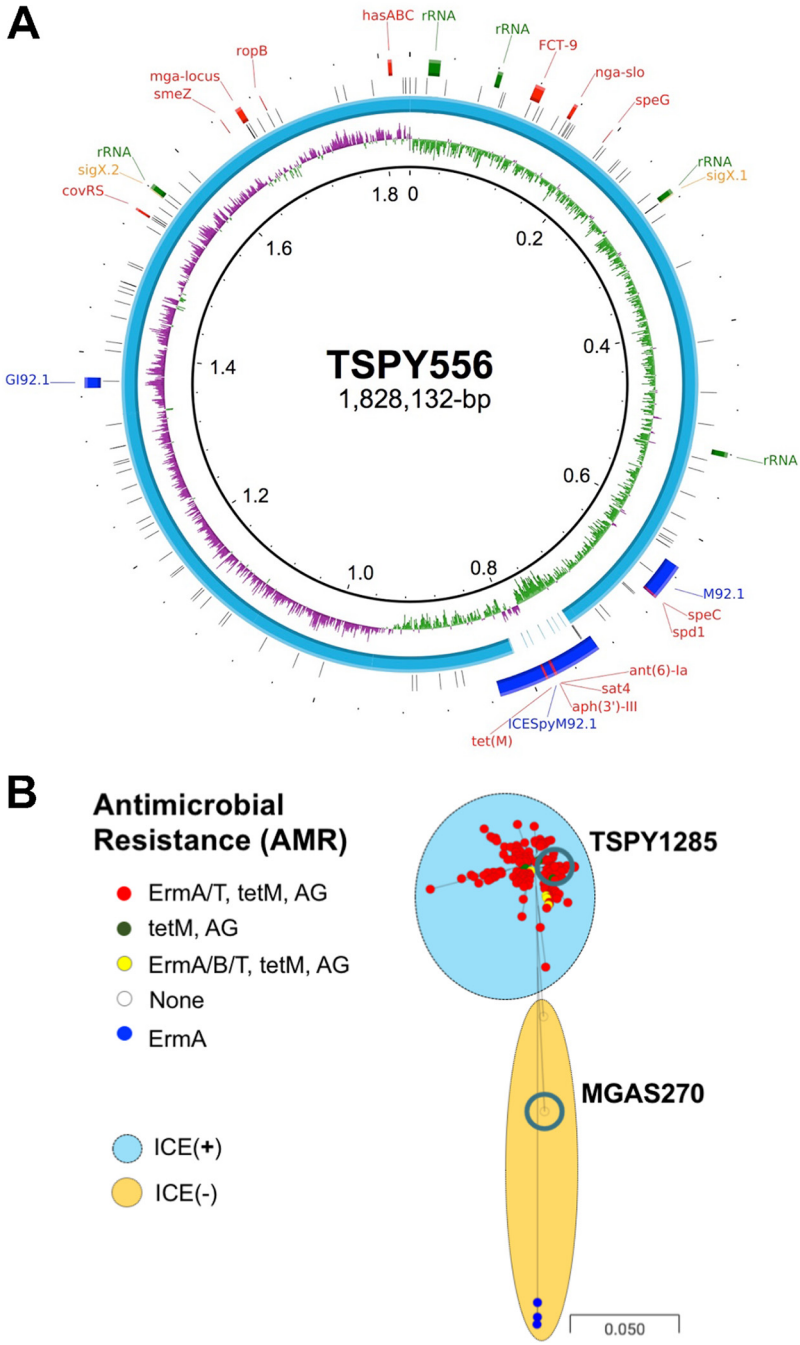

FIG 1 Emergent *emm92* constitutes a highly clonal population in which ICESpyM92 is well conserved, suggesting recent emergence. (A) Comparison of MGAS270 whole genome sequence to emergent *emm92* reference genome (TSPY556; accession no. CP032700). Rings denote (from innermost to outermost), genome position in Mb (ring 1), GC skew (ring 2), blast comparison of MGAS270 relative to TSPY556 (ring 3), polymorphisms (SNPs/Indels) in MGAS270 relative to TSPY556 (ring 4), and chromosomal features of TSPY556 reference genome (ring 5). Chromosomal features are color-coded as follows: blue = mobile genetic elements (MGEs), red = annotated virulence and antimicrobial resistance (AMR) genes [*tet*(M), *aph(3′)-III*, *sat4*, and *ant(6)-Ia*], green = rRNA operons, and yellow = sigX site of genome inversion. Note absence of AMR-encoding ICESpyM92 MGE in MGAS270 whole genome sequence. (B) Phylogenetic reconstruction using 901 core biallelic SNP loci of invasive *emm92* from Houston (n = 19), Centers for Disease Control Active Bacterial Core surveillance (n = 239) and the MGAS270 strain, relative to the reference genome TSPY556. Node color indicates AMR genotype for aminoglycosides (AG), macrolides (ErmA/B/T), and tetracycline (tetM). Shaded ovals denote nodes corresponding to ICE(+) and ICE(–) strains. Nodes corresponding to TSPY1285 and MGAS270 strains (circled in gray) are indicated. Phylogenetic tree is rooted in strain TSPY556.

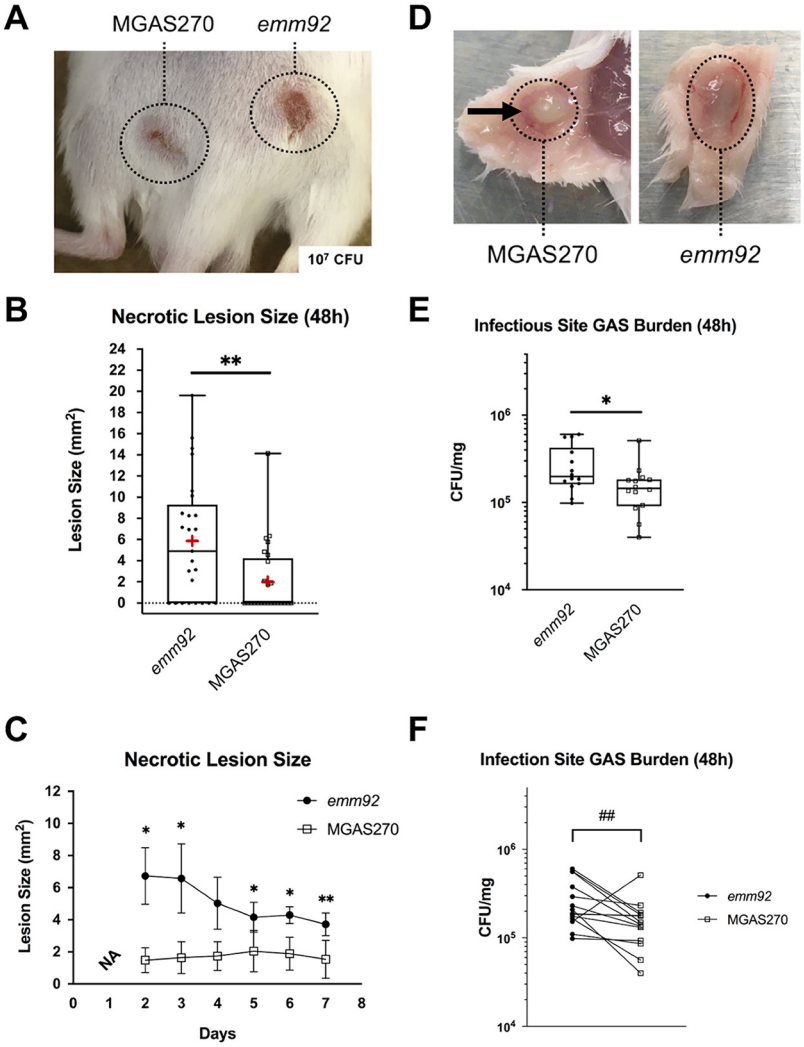

FIG 2 Emergent *emm92* GAS exhibits enhanced virulence in a murine model of SSTI. Individual mice infected subcutaneously in flanks (contralaterally) with ICE(–) MGAS270 and ICE(+) emergent *emm92* (TSPY1285) streptococcal strains (10^7 CFU) exhibit necrotic lesion development at 48 hpi. (A) Dashed lines indicate area of infection site; image representative of observed necrotic lesion phenotype. (B) Size of necrotic lesion (mm^2) at sites of emergent *emm92* and MGAS270 infection measured at 48 hpi. The mean (red cross) and median lesion size with 95% confidence interval (box and whisker plot) are indicated. Symbols represent necrotic lesion size in individual mice. (C) Size of necrotic lesion (mm^2) at sites of emergent *emm92* and MGAS270 infection measured at daily time points postinfection. The mean lesion size (symbols) and SEM (error bars) are indicated. Necrotic lesions were not visible at 1day postinfection (NA). Statistically significant differences in lesion size at each time point are indicated. (D) Representative images of dermal tissue excised from mouse infections sites (interior face of dermis shown). Area of inflammation associated with infection outlined in dashed lines. Infectious site abscess at MGAS270 infection site indicated (arrow). (E and F) Infectious site burden of emergent *emm92* and MGAS270 quantified as CFU/mg of homogenized infected tissue at 48 hpi. Median burden and 95% confidence interval (box and whisker plot) (E), as well as paired comparisons (F) of infectious site emergent *emm92* and MGAS270 burdens are indicated. Symbols represent individual infection site burden and lines connect infection site burdens of individual mice. Figure legends indicate symbol correspondence to infecting strain. Statistical significance was determined by Mann-Whitney U-test (**, $P < 0.01$; *, $P < 0.05$) or by Wilcoxon signed-rank test (##, $P < 0.01$).

diffuse tissue inflammation was apparent at ICE(+) infection sites (Fig. 2D). The median burden of GAS at the emergent *emm92* infection site was also significantly greater than at the MGAS270 site at 48 hpi (Fig. 2E; $P = 0.0274$). This difference was also statistically significant in paired comparisons of the GAS burden at the infection sites in individual mice (Fig. 2F; $P = 0.0067$). These results indicate that ICE(+) emergent *emm92* is more virulent than the historical ICE(–) MGAS270 in SSTI.

Presence of ICESpyM92 alters GAS virulence in mouse models of streptococcal infection. To further test the hypothesis that ICESpyM92 contributes to emergent *emm92* virulence, we next generated isogenic ICE(+) and ICE(–) mutants of MGAS270 and emergent *emm92* strains, respectively, for comparison in the mouse subcutaneous infection model. The ICESpyM92-complemented strain (*MGAS270*$^{+ICE}$) encodes ICESpyM92 immediately downstream of a 23S rRNA uridine methyltransferase (*rlmD*), the same gene locus (D8S77_03855) at which the ICE is located in emergent *emm92* (Fig. 1A). Multiple attempts to generate an ICESpyM92-negative mutant (Δ*ICE*) in the emergent *emm92* isolate TSPY1285 were unsuccessful. However, we were able to do so in the reference emergent *emm92* strain, TSPY556 (Fig. 1). TSPY556 and TSPY1285 differ by only 6 single nucleotide polymorphisms (SNPs), including a nonsynonymous SNP resulting in an amino acid mutation at position 272 in the CovS sensor kinase of TSPY556. CovRS two-component system polymorphisms have been associated with virulence-related phenotypic differences (17), such as in capsule production observed in TSPY556 relative to MGAS270 and TSPY1285 in our initial studies (Supplemental Methods, Fig. S1). Mutagenesis of the SNP in the *covS*^{S272L} allele reverted this phenotype (strain JMF1026, Fig. S1). Examination of emergent *emm92* sequenced genomes (n = 263) determined CovRS polymorphisms are present in only 29 emergent *emm92* strains (11%), a frequency comparable to that observed among other sequenced invasive GAS isolates (18), suggesting CovRS mutation does not define emergent *emm92*.

Using the newly generated isogenic strains (emergent *emm92* strain JMF1026 and Δ*ICE*; MGAS270 and *MGAS270*$^{+ICE}$), mice were infected at a lower infectious dose (10^6 CFU) to better assess, in addition to virulence, the ICE-associated capacity of emergent *emm92* strains to establish infection. Median necrotic lesion size 48 hpi was significantly greater at the site infected with *MGAS270*$^{+ICE}$ than the site infected with the isogenic ICE(–) parent strain (MGAS270; P = 0.0222) (Fig. 3A). Though not statistically significant, similar differences were observed between the Δ*ICE* strain and its isogenic parent, as well as between the emergent *emm92* strain and MGAS270 (P = 0.069). As observed using TSPY1285, the median GAS burden at 48 hpi was highest in the emergent *emm92*-infected site and significantly higher than in the sites infected by the MGAS270 and *MGAS270*$^{+ICE}$ (P = 0.001 and P = 0.0361, respectively) (Fig. 3B). Paired comparisons of GAS burden at infection sites in individual mice indicate statistically significant differences between ICE(+) and ICE(–) isogenic strain pairs (Wilcoxon, *emm92* versus Δ*ICE*: P = 0.0166, MGAS270 versus *MGAS270*$^{+ICE}$: P = 0.0245) (Fig. 3C). These results suggest that the presence of ICESpyM92 contributes to SSTI and promotes necrotic lesion development.

Histopathological comparison in individual mice of emergent *emm92* strain JMF1026 and historical MGAS270 infection sites revealed contrasting patterns of tissue damage, even at a lower infectious dose (10^6 CFU; Fig. S2). The MGAS270-infected sites exhibit formation of a well-defined abscess and limited tissue damage (Fig. S2C), whereas the emergent *emm92* infected site shows extensive necrosis, breakdown of skin layers and greater dissemination of infection (Fig. S2E). Similar phenotypes were observed when comparing MGAS270-infected sites (Fig. S2D) with isogenic ICE(+) *MGAS270*$^{+ICE}$-infected sites (Fig. S2F) in individual contralaterally infected mice.

We additionally compared the virulence of ICE(+) and ICE(–) isogenic strain pairs in a murine intraperitoneal model of invasive infection. An emergent *emm92* infectious dose of 10^8 CFU resulted in 50% survival of tested mice (n = 10) over a 72-h experimental period, whereas an equivalent dose of Δ*ICE* GAS produced a lower level of lethality (Fig. 3D). Conversely, infection with *MGAS270*$^{+ICE}$ resulted in reduced survival of mice relative to infection with the isogenic ICE(–) parent strain. The difference in survival was statistically significant between emergent *emm92* and MGAS270 strains (P = 0.0115), further evincing the enhanced virulence of emergent *emm92*. The differences in survival between isogenic ICE(+) and ICE(–) strains trended similarly and, though not statistically significant (P = 0.146), suggest that the presence of ICESpyM92 may contribute to GAS pathogenicity. Differences in GAS burden in the harvested spleens (Fig. 3E) of intraperitoneally infected mice similarly demonstrate the enhanced virulence of emergent *emm92*. The median GAS burden in the spleens of emergent *emm92*-infected mice was

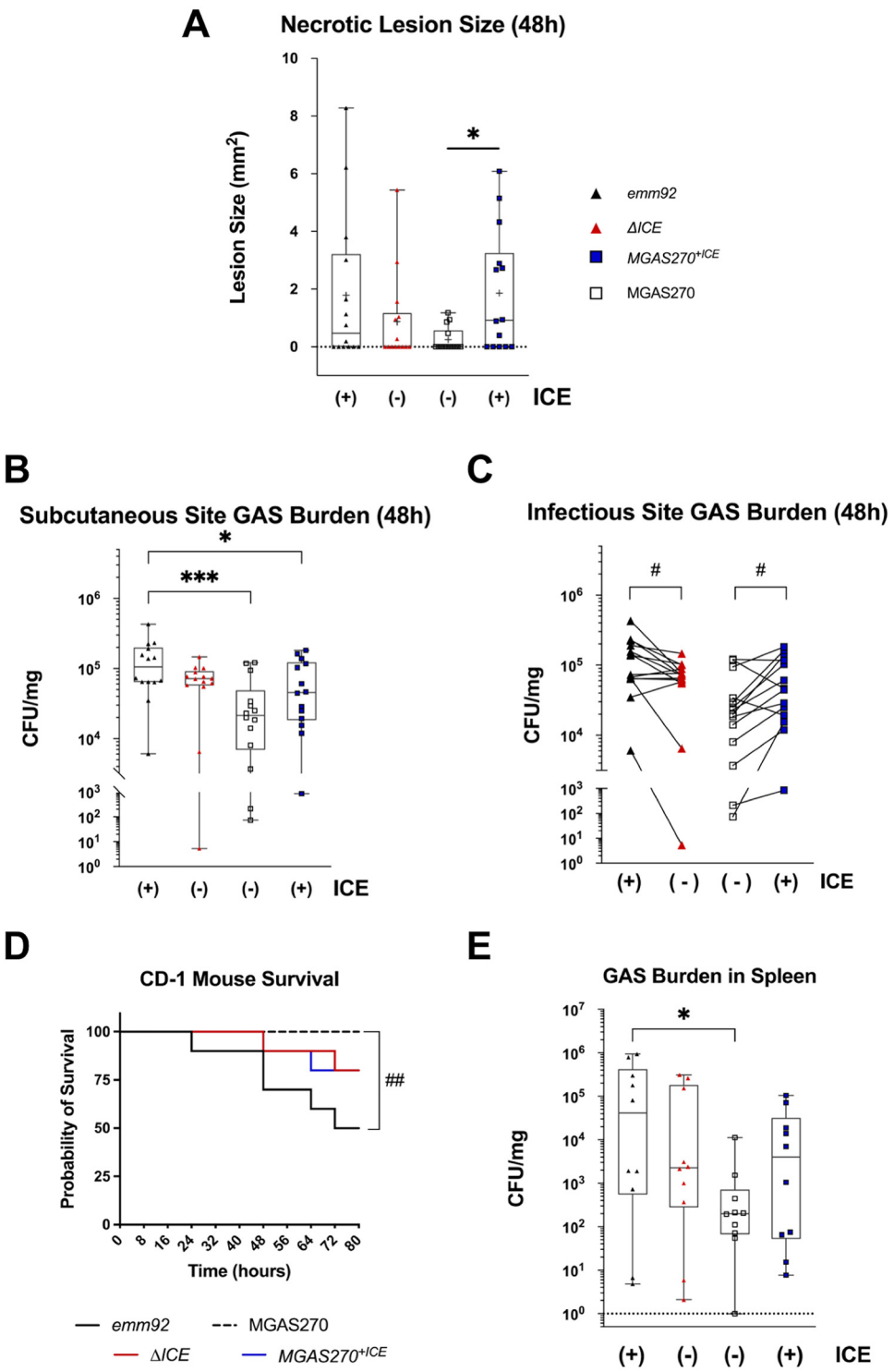

FIG 3 ICESpyM92 contributes to enhanced virulence in a murine model of SSTI. Individual mice infected subcutaneously in flanks (contralaterally) with isogenic ICE(+) and ICE(–) strain pairs (emergent *emm92* [JMF1026] versus Δ*ICE* and *MGAS270*$^{+ICE}$ versus MGAS270; 10^6 CFU) exhibit ICESpyM92-related statistically significant differences in necrotic lesion development and bacterial burden at 48 hpi. (A) Size of necrotic lesion (mm^2) at sites of infection measured at 48 hpi. The mean (gray cross) and median lesion size with 95% confidence interval (box and whisker plot) are indicated. Symbols represent necrotic lesion size in individual mice. (B and C) Infectious site GAS burden quantified as CFU/mg of homogenized infected tissue at 48 hpi. Median GAS burden and 95% confidence interval (box and whisker plot) (B) as well as paired comparisons of isogenic ICE(+) and ICE(–) infectious site burdens in individual mice (C) are indicated. (D) Kaplan-Meier survival curves of CD-1 mice (n = 10 per strain) infected intraperitoneally with isogenic ICE(+) and ICE(–) strain pairs

(Continued on next page)

significantly higher (~200-fold, $P = 0.0355$) than in MGAS270-infected mice. The median burden of Δ*ICE* was lower (~18-fold) than that of its isogenic ICE(+) parent strain, whereas that of *MGAS270*$^{+ICE}$ was higher (~20-fold) than that of MGAS270 (Fig. 3E). Although the differences between isogenic ICE mutant strains were not statistically significant, the similar trends of reduced host survival and higher GAS burdens associated with strains encoding ICESpyM92 would suggest contribution of the ICE to GAS virulence.

Presence of ICESpyM92 contributes to *in vitro* differential gene expression. To this point we had observed that ICESpyM92, which does not encode any known GAS virulence genes, contributes to emergent *emm92* virulence in a murine model in the absence of antimicrobials. The predicted open reading frames (ORFs) of ICESpyM92 include multiple transcriptional regulators associated with a secretion/conjugation system, AMR genes, and genes of unknown function (Table S3). Evidence suggests that the presence of MGEs lacking AMR genes may influence the GAS transcriptome (8, 19). We hypothesized that the presence of ICESpyM92 alters GAS global gene expression. We first tested this hypothesis by performing *in vitro* RNA-seq analysis of isogenic ICE(+) and ICE(–) strains to determine differential gene expression (DGE) patterns associated with the presence of ICESpyM92 in emergent *emm92* and MGAS270 genomic backgrounds. No differences in rate of growth *in vitro* were observed across isogenic ICE(+) and ICE(–) strain pairs (Fig. S3). Compared to ICE(–) strains, 60 and 210 transcripts were differentially expressed (>1.5-fold, $P < 0.05$) in the presence of ICESpyM92 in the emergent *emm92* (Fig. 4A, Table 1, and Table S4) and MGAS270 (Table S5) genomic backgrounds, respectively. Of these, 44 transcripts showed concordant DGE patterns in both strain backgrounds in the presence of ICESpyM92, suggesting their differential expression is ICE-dependent (Fig. 4A and Table 1).

Among the transcripts that were upregulated in an ICESpyM92-dependent manner, the lactose utilization operon (*lacA.1-lacD.1*), lactate oxidase (*lctO*), and arginine-deiminase (ADI) pathway components (i.e., *arcA*, *argF/arcB*) exhibited the greatest difference in expression levels (Fig. 4B). The transcript levels of *speB* and *spyCEP*, which encode immunomodulating GAS proteases involved in virulence, were also increased. Transcripts downregulated in the presence ICESpyM92 included components of the inosine-monophosphate pathway of purine synthesis (e.g., *purN*, *purH*). Carbohydrate and amino acid import/metabolism transcripts (e.g., *pfkB/fruB*, galactose PTS, and ABC transporters) (Fig. 4B) were also differentially expressed and constituted a major part of DGE observed in the presence of ICESpyM92 in the MGAS270 genomic background (Table S5). These results suggest ICESpyM92-associated DGE alters metabolic and virulence patterns that may in turn influence emergent *emm92* infection of the host skin niche.

In vivo data (i.e., emergent *emm92* burden relative to MGAS270 and *MGAS270*$^{+ICE}$) (Fig. 3B) suggest core genome transcription differences independent of ICESpyM92 may contribute to disease phenotype. Thus, we also examined DGE in emergent *emm92* relative to historical MGAS270. Comparison of *in vitro* DGE in the emergent *emm92* and isogenic Δ*ICE* strains relative to MGAS270 revealed that 56 transcripts were differentially expressed in the emergent *emm92* background, independently of ICESpyM92 presence (Fig. 4C and Table 2). Several of these transcripts are associated with GAS virulence, encoding adherent and immunomodulatory proteins (*emm*, *scpA*, *sclA*, *sof*, *sfbX*, *fbpA*, and *grab*) as well as cytotoxins (*nga* and *slo*). Significant differential expression of *spyCEP* and *purN* transcripts in the *emm92* background relative to MGAS270 was also observed. These data suggest that there are also core genomic differences in

FIG 3 Legend (Continued)

(10^8 CFU). (E) GAS burden in spleens of intraperitoneally-infected mice, quantified as CFU/mg of homogenized tissue at time test subjects were euthanized. Median GAS burden and 95% confidence interval (box and whisker plot) are indicated. Symbols represent GAS burden in individual mice. Figure legend indicates symbol/color correspondence to infecting strain. Statistical significance was determined by Mann-Whitney U-test (***, $P < 0.001$; *, $P < 0.05$), Wilcoxon signed-rank test (#, $P < 0.05$), or by Mantel-Cox log rank test (##, $P < 0.05$).

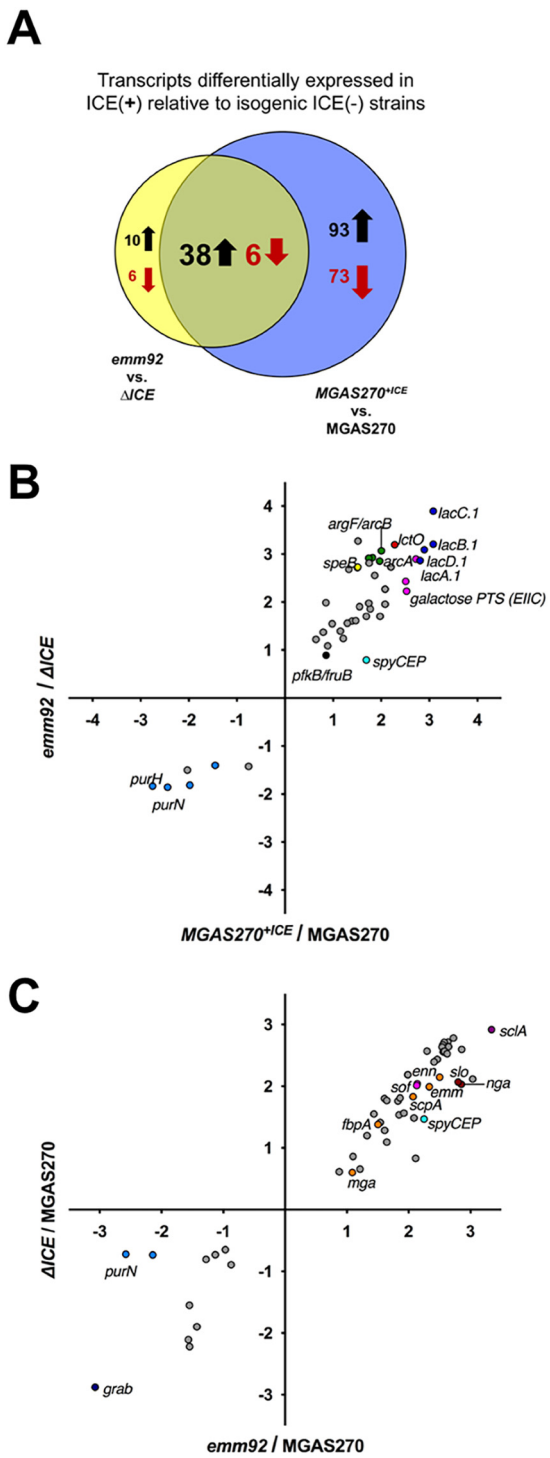

FIG 4 Presence of ICESpyM92 contributes to *in vitro* differential gene expression (DGE). RNAseq analysis of isogenic ICE (+) and ICE(–) transcriptomes (emergent *emm92* ([JMF1026] versus Δ*ICE* and *MGAS270*$^{+ICE}$ versus MGAS270) during exponential growth *in vitro* (THY medium) revealed ICE-related DGE. (A) Diagram illustrating the number of transcripts upregulated (black) and downregulated (red) in ICE(+) relative to isogenic ICE(–) transcriptomes in the emergent *emm92* (yellow circle) and the MGAS270 background (blue circle). Overlapping region indicates number of transcripts similarly differentially expressed in both ICE(+) transcriptomes. (B) Correlation plot of 44 significantly ($P < 0.05$; Bonferroni correction) differentially expressed genes (≥1.5-fold relative to ICE[–] isogenic strain) shared between the *MGAS270*$^{+ICE}$ (*x* axis) and the emergent *emm92* (*y* axis) transcriptome. (C) Correlation plot of 56 significantly ($P < 0.05$, Bonferroni correction) differentially expressed genes (≥1.5-fold relative to ICE[–] MGAS270 strain) shared between the emergent *emm92* (*x* axis) and the isogenic Δ*ICE* (*y* axis) transcriptome. Log_2 values are plotted, colors correspond to gene operons and names of virulence genes of interest are listed.

TABLE 1 GAS transcript differential expression *in vitro* associated with the presence of ICESpyM92 in emergent *emm92* and MGAS270

			Log$_2$ fold change	
Accession no.[a]	Name	Product	Emergent *emm92*[b]	*MGAS270*$^{+ICE}$ [c]
D8S77_00280	*purF*	Amidophosphoribosyltransferase	−1.40	−1.45
D8S77_00285	*purM*	Phosphoribosylformylglycinamidine cyclo-ligase	−1.81	−1.98
D8S77_00290	*purN*	Phosphoribosylglycinamide formyltransferase	−1.85	−2.44
D8S77_00295	*purH*	Bifunctional phosphoribosylaminoimidazolecarboxamide formyltransferase	−1.83	−2.75
D8S77_02295		Galactose PTS sugar transporter subunit EIIA	2.43	2.51
D8S77_02300		Galactose PTS sugar transporter subunit EIIB	2.90	2.72
D8S77_02305		PTS Galactose transporter subunit EIIC	2.23	2.53
D8S77_02310	*lacA.1*	Galactose-6-phosphate isomerase subunit LacA	2.87	2.81
D8S77_02315	*lacB.1*	Galactose-6-phosphate isomerase subunit LacB	3.21	3.08
D8S77_02320	*lacC.1*	Tagatose-6-phosphate kinase	3.89	3.08
D8S77_02325	*lacD.1*	Tagatose-bisphosphate aldolase	3.09	2.90
D8S77_02995	*arcA*	Arginine deiminase	2.86	1.97
D8S77_03000		GNAT family N-acetyltransferase	2.93	1.82
D8S77_03005	*argF/arcB*	Ornithine carbamoyltransferase	3.07	2.00
D8S77_03010	*arcD*	YfcC family protein/arginine/ornithine antiporter	2.92	1.74
D8S77_03015	*arcT*	Sapep family Mn(2+)-dependent dipeptidase	2.72	1.51
D8S77_05965	*pfkB/fruB*	1-phosphofructokinase	0.89	0.85
D8S77_07560	*spyCEP*	Immunomodulating cell envelope protease	0.79	1.69
D8S77_07565	*lctO*	L-lactate oxidase	3.20	2.28
D8S77_08555	*speB*	Pyrogenic exotoxin B	2.73	1.51

[a]Reference genome TSPY556 (NCBI: CP032700.1).
[b]Differential gene expression in *emm92* (JMF1026) relative to Δ*ICE* isogenic mutant.
[c]Differential gene expression in *MGAS270*$^{+ICE}$ mutant relative to MGAS270 isogenic parent.

emergent *emm92* strains contributing to their enhanced skin pathogenicity relative to MGAS270.

Emergent *emm92* transcripts exhibit ICE-associated and ICE-independent differential expression in the context of interaction with human epithelial keratinocytes. Our data to this point indicate gene expression differences *in vitro* associated with the presence of ICESpyM92. To provide further evidence supporting our hypothesis that ICESpyM92 influences GAS gene expression and in turn virulence, we measured DGE in an *ex vivo* model of GAS infection. Emergent *emm92* are nearly exclusively isolated from SSTI. We therefore selected cultured human primary epithelial keratinocytes (HEK) to assess ICE-related GAS DGE. We measured the transcript levels of targets of interest (Fig. 4) in isogenic ICE(+) and ICE(–) strains adherent to HEK. Of the transcripts examined, *lctO*, *emm*, and *slo* showed significant, ICE-related, increased expression (>1.5-fold, $P < 0.01$) (Fig. 5A). Differential expression of targets was only detected in the emergent *emm92* strain background, as increased expression of *slo* in *MGAS270*$^{+ICE}$ relative to its isogenic parent was not statistically significant (Fig. 5B).

Comparison of target levels in ICE(+) and ICE(–) strains in the emergent *emm92* background relative to MGAS270 (Fig. 5C) and in emergent *emm92* relative to *MGAS270*$^{+ICE}$ (Fig. 5D) show that significantly enhanced *lctO* expression in the emergent *emm92* background correlated with the presence of ICESpyM92 ($P < 0.05$). In contrast to our *in vitro* observations, statistically significant differences in *arcA* transcript levels were not detected (Fig. 5A and B). On the other hand, levels of *emm* and *slo* transcripts in the emergent *emm92* background relative to MGAS270 (Fig. 5C) and *MGAS270*$^{+ICE}$ (Fig. 5D) indicate that both ICESpyM92 and strain background significantly influence expression of these targets in the context of interaction with HEK ($P < 0.05$). In contrast, significantly increased *spyCEP* expression in emergent *emm92* relative to the MGAS270 background appears to be independent of ICESpyM92 ($P < 0.05$) (Fig. 5C and D). These results suggest that ICESpyM92 influences DGE in a background-dependent manner.

DISCUSSION

We previously described the association of GAS derived from invasive disease with emerging resistance to second-line antimicrobials (12). That study found that closely

TABLE 2 Emergent *emm92* transcripts differentially expressed *in vitro* relative to MGAS270, independently of the presence of ICESpyM92

			Log$_2$ fold change[b]	
Accession no.[a]	Name	Product	*emm92*	Δ*ICE*
D8S77_00280	***purF***	**Amidophosphoribosyltransferase**	**−2.14**	**−0.73**
D8S77_00290	***purN***	**Phosphoribosylglycinamide formyltransferase**	**−2.58**	**−0.72**
D8S77_00810		Hypothetical protein	1.10	0.86
D8S77_00850	*sloR*	Transcriptional regulator (environmental sensing/metabolism)	1.21	0.66
D8S77_00925	***nga***	**N-acetylglucosamine-1-phosphate uridyltransferase**	**2.85**	**2.03**
D8S77_00930	***ifs***	**NAD glycohydrolase inhibitor**	**3.04**	**2.12**
D8S77_00935	***slo***	**Cholesterol-dependent cytolysin streptolysin O**	**2.80**	**2.07**
D8S77_00945		Hypothetical protein	2.86	2.60
D8S77_00950		Hypothetical protein	2.09	1.49
D8S77_00955		Hypothetical protein	1.84	1.53
D8S77_01975		NisF family ABC transporter ATP-binding protein	1.33	1.20
D8S77_02435		Bacteriocin immunity protein	−1.54	−2.22
D8S77_02440		ABC transporter ATP-binding protein	−1.43	−1.90
D8S77_02445	*proB*	ABC transporter permease	−1.57	−2.11
D8S77_03360		HNH endonuclease	1.54	1.41
D8S77_03365		Hypothetical protein	1.61	1.29
D8S77_03370		Phage portal protein	1.61	1.80
D8S77_03395		Phage terminase	2.73	2.78
D8S77_03400		DUF4355 domain-containing protein	2.64	2.72
D8S77_03405		Phage major capsid protein	2.58	2.72
D8S77_03410		Hypothetical protein	1.98	2.19
D8S77_03415		Hypothetical protein	2.59	2.63
D8S77_03420		Hypothetical protein	2.55	2.67
D8S77_03425		Hypothetical protein	2.30	2.57
D8S77_03430		Hypothetical protein	2.54	2.64
D8S77_03435		Phage tail protein	2.65	2.64
D8S77_03440		Hypothetical protein	2.56	2.56
D8S77_03445		Hypothetical protein	2.58	2.57
D8S77_03450	*pblA*	Putative human platelet-binding protein, phage-associated	2.46	2.44
D8S77_03455		Hypothetical protein	2.62	2.53
D8S77_03460	*pblB*	Peptidase/putative platelet-binding protein - phage-associated	1.83	1.76
D8S77_03470		Hypothetical protein	2.41	2.39
D8S77_03480		DUF1366 domain-containing protein	−0.87	−0.89
D8S77_03515	*pyrD*	Dihydroorotate oxidase	−1.13	−0.73
D8S77_03815	***grab***	**α2macroglobulin-binding protein**	**−3.07**	**−2.88**
D8S77_04225		MFS transporter	−1.55	−1.55
D8S77_04475		Sodium:alanine symporter family protein	−0.97	−0.65
D8S77_06075	*pyrR*	Bifunctional pyrimidine operon transcriptional regulator/uracil phosphoribosyltransferase	−1.28	−0.81
D8S77_07470		Hypothetical protein	1.92	1.57
D8S77_07485		Hypothetical protein	1.65	1.77
D8S77_07490		Hypothetical protein	1.86	1.81
D8S77_07500		Hypothetical protein	2.48	−1.20
D8S77_07510		Hypothetical protein	2.11	0.83
D8S77_07560	***spyCEP***	**Immunomodulating cell envelope protease**	**2.25**	**1.47**
D8S77_08330	***sclA***	**Streptococcal collagen-like surface adhesin**	**3.34**	**2.92**
D8S77_08445	***fbpA***	**Fibronectin binding protein**	**1.51**	**1.38**
D8S77_08450	***scpA***	**C5 peptidase**	**2.07**	**1.83**
D8S77_08455	***enn***	**M-like protein**	**2.50**	**2.15**
D8S77_08460	***emm***	**M protein**	**2.34**	**1.99**
D8S77_08470	***mga***	**M protein trans-acting positive regulator**	**1.09**	**0.60**
D8S77_08525	***sfbX***	**Fibronectin binding protein**	**2.14**	**2.04**
D8S77_08530	***sof***	**Serum opacity factor**	**2.13**	**2.01**
D8S77_08535		Hypothetical protein	1.65	1.09
D8S77_09095	*sdaAA*	L-serine ammonia-lyase, iron-sulfur-dependent, subunit alpha	0.88	0.61
D8S77_09215		IS30 family transposase	1.44	1.55

[a]TSPY556 genome sequence (NCBI: CP032700.1).
[b]Differential gene expression in emergent *emm92* (JFM1026) and isogenic Δ*ICE* mutant relative to MGAS270 strain. Bolded text denotes virulence genes of interest.

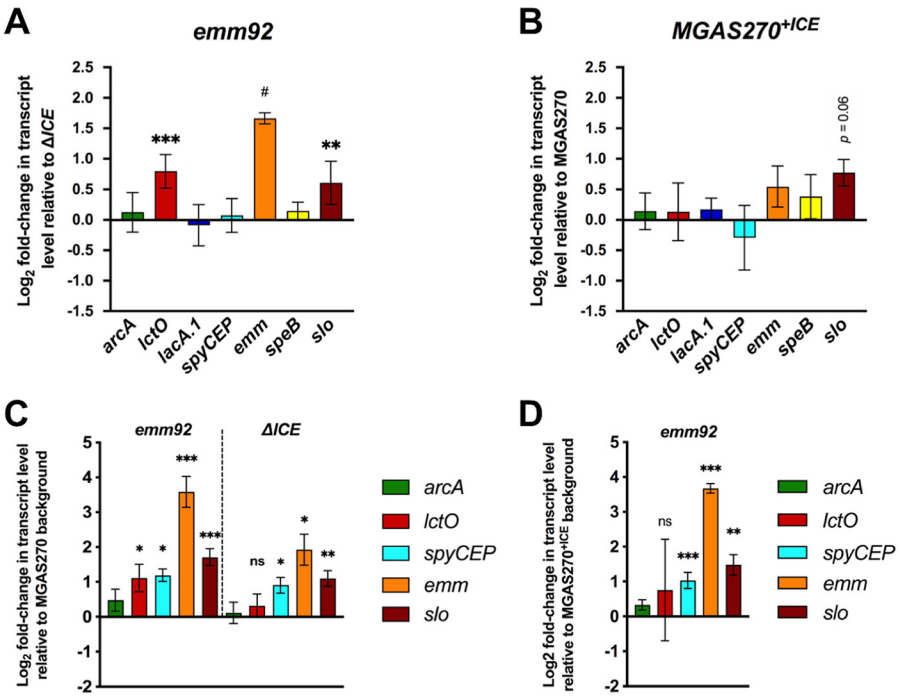

FIG 5 Emergent emm92 transcripts exhibit ICE-related and ICE-independent differential expression in the context of interaction with human epithelial keratinocytes. Differential expression of selected targets in ICE(+) relative to isogenic ICE(–) strains (A) emergent *emm92* relative to Δ*ICE* and (B) in *MGAS270*$^{+ICE}$ relative to MGAS270 adherent to human epithelial keratinocytes (HEK) measured by quantitative real-time PCR (qRT-PCR). (C) Differential expression of selected targets in the emergent *emm92* background relative to the historical MGAS270 genomic background (i.e., emergent *emm92* and isogenic Δ*ICE* relative to MGAS270) and (D) in the emergent *emm92* background relative to the ICE(+) historical mutant (*MGAS270*$^{+ICE}$) adherent to HEK measured by qRT-PCR. Compared GAS strains were allowed to adhere to HEK (MOI 100:1), grown for 2 h in biological quadruplicate and transcript levels were measured in triplicate for each target. Mean Log_2 fold change in transcript level relative to comparison strain is plotted (*y* axis) with 95% confidence interval (error bars) for each gene target (*x* axis). Differentially expressed genes (≥1.5-fold relative to comparison strain) and statistical significance are indicated (#, $P < 0.0001$; ***, $P < 0.001$; **, $P < 0.01$; *, $P < 0.05$; ns = not significant; Student's *t* test).

related *emm92* strains (emergent *emm92*), resistant to multiple antimicrobials and isolated with increasing frequency during the study period (2015–2017), were obtained nearly exclusively from invasive or skin and soft tissue infections (SSTI). We hypothesized ICESpyM92 – responsible for aminoglycoside and tetracycline resistance in emergent *emm92* strains – contributed to GAS pathogenicity. The data presented support this hypothesis and provide evidence that a combination of ICESpyM92- and core genome-dependent differential gene expression contributes to invasive disease phenotypes in emergent *emm92* GAS. Tested emergent *emm92* strains exhibited greater virulence in mouse subcutaneous and intraperitoneal infection models than the antimicrobial-susceptible invasive isolate MGAS270, decreasing survival and generating significantly greater infectious burdens at distinct infectious doses (10^6–10^8 CFU). Measured differences in necrotic lesion size indicate enhanced invasiveness and tissue destruction by an emergent *emm92* strain. *In vivo* virulence phenotype trends associated with the presence of ICESpyM92 suggest that ICE contributes to *emm92* virulence and likely in conjunction with core genomic differences between emergent *emm92* and the historical MGAS270 strain. Significantly enhanced necrotic lesion formation and increased infection site GAS burden resulting from introduction of ICESpyM92 into the historical MGAS270 background suggest ICESpyM92 contribution to virulence is dependent on genomic background. Our transcriptomic results *in vitro* and in GAS interaction with HEK indicate that gene expression in emergent AMR *emm92* is distinct from that in an antimicrobial-susceptible *emm92* strain, both in an ICE-related and independent manner.

Our results add to research defining the contribution of MGEs to bacterial disease potential by linking ICE-related DGE and virulence with AMR on a unique MGE. Previous research had shown that bacteriophage encoding virulence factors (e.g., DNase, superantigens) can enhance virulence of GAS involved in disease outbreaks while, independently, AMR-encoding ICEs may increase their drug resistance (20). The RD2 element, encoding no AMR, was shown to enhance *emm28* vaginal colonization in mice (8). RD2-conjugants in other genomic backgrounds displayed a similar phenotype (9). Furthermore, presence of RD2 influenced expression of >100 core chromosomal GAS genes in a serotype-dependent manner (8, 9). Our research shows that, unlike previously described MGEs of GAS, ICESpyM92 both confers high-level AMR (12) and has the potential to enhance *emm92* virulence through alteration of the GAS transcriptome. Jain et al. hypothesize RD2-encoded transcriptional regulators are responsible for changes in core chromosomal GAS gene expression (8). Like RD2, ICESpyM92 encodes multiple transcriptional regulators associated with a secretion/conjugation system, AMR genes, and genes of unknown function. Alternatively, the prophage-like *SpyCIM1* altered virulence and metabolism gene expression in an *emm1* strain during exponential growth, when *SpyCIM1* is episomal to the GAS chromosome (19). The mechanism by which ICESpyM92 gene content affects DGE is not presently known and is of interest for further investigation.

ICESpyM92-related DGE and influence on virulence appear to be dependent on genomic background. In both *in vivo* infectious models, the presence of ICESpyM92 more visibly influenced virulence and GAS burden in the MGAS270 background. Likewise, ICESpyM92 did not have the same effect on *ex vivo* transcript levels in the MGAS270 background as in an emergent *emm92* strain. Furthermore, *emm* and *slo* transcript levels of tested emergent *emm92* and an isogenic Δ*ICE* mutant relative to MGAS270 indicate that ICESpyM92 and core chromosomal gene content have a combined effect on DGE. The differences in ICE-related DGE *in vitro* between the two genomic backgrounds examined (i.e., 60 transcripts in an emergent *emm92* strain versus 210 in MGAS270) is further evidence that the conjunction of distinct core chromosomal traits with MGE content produces substantial variation in the GAS transcriptome. Altered *in vitro* expression of known GAS virulence genes (*scpA*, *sclA*, *sof*, *sfbX*, *fbpA*, *grab*, *nga*, and *spyCEP*) in an emergent *emm92* isolate relative to MGAS270, independently of ICESpyM92, suggest that DGE solely related to core chromosomal differences may be contributing to emergent *emm92* virulence as well. This is supported by the enhanced *spyCEP* transcript levels in the course of HEK adherence, irrespective of ICESpyM92 presence. Core chromosomal differences in emergent *emm92* that contribute to altered gene expression and virulence relative to MGAS270 remain to be investigated.

ICESpyM92-related DGE suggests the ICE may influence GAS adaptation to stressors in the SSTI niche. Lactate oxidase (*lctO*) mediates lactate metabolism and endogenous hydrogen peroxide (H_2O_2) production, which varies widely across GAS *emm* types with distinct disease potential (21). Differential expression of *lctO* is involved in GAS colonization of invasive infection models (22, 23). The arginine deiminase pathway has been shown to enhance GAS virulence in animal models of invasive infection (24–26) through modulation of host immunity (27). Differential expression of GAS transcripts (*emm* and *slo*) directly involved in immune evasion and cytotoxicity in the course of invasive disease (28), further suggest the ICE may influence emergent *emm92* resistance to stress from host immune cells. Phenotypes such as H_2O_2 production, cytotoxicity and resistance to immune cell challenge will be explored in the future to define how ICESpyM92-related DGE contributes to emergent *emm92* virulence.

It is highly unlikely that antimicrobial pressure alone can explain the maintenance of ICESpyM92 within currently circulating and increasingly frequent invasive *emm92* strains. AMR gene maintenance and dissemination by ICEs potentially involves associations with virulence determinants, as suggested by the correlation of virulence and AMR gene diversity in human gut microbiomes, independently of geographic origin, despite prominent

differences in antimicrobial use (29). There is also evidence to support a role for virulence factors in AMR maintenance from specific instances in which genes contributing to virulence (1, 30) or fitness (31) correlate with AMR. Importantly, ICESpyM92 may not be the only AMR-encoding MGE contributing to GAS pathogenicity. Our previous study showed AMR in invasive disease-related *emm77* and *emm11* strains is encoded on well-conserved ICEs and transposons, respectively (12).

The presence of ICESpyM92 does not appear to be the only contributing factor to enhanced virulence of emergent *emm92*. Our data show a core genome-dependent level of virulence associated with the emergent *emm92* background. The paucity of temporally distant *emm92* strains available for comparison limits our ability to define the core genomic differences, in addition to the presence of ICESpyM92, that contribute to emergent *emm92* isolate association with SSTIs. Although our direct comparisons were limited to individual historical and emergent *emm92* strains, the close-relatedness of emergent *emm92* described by our previous study suggests transcriptomic and phenotypic differences described herein may be illustrative of shared traits among increasingly frequent AMR *emm92* (32). Furthermore, our work highlights the importance of investigating associations between AMR-encoding MGEs, their genomic background, and pathogenicity, not just in GAS but in other pathogenic bacteria as well. Association of resistance and virulence phenotypes within MGEs in pathogenic GAS strains constitutes a concerning epidemiological threat that necessitates continued surveillance and further investigation of AMR patterns and disease phenotypes across GAS serotypes.

MATERIALS AND METHODS

Bacterial strains and culture conditions. The strains used in this study are listed in Table S1. GAS was grown in Todd-Hewitt broth containing 0.2% (wt/vol) yeast extract (THY; Difco Laboratories), on THY agar, and Trypticase soy agar containing 5% sheep blood (SBA; Becton, Dickinson), as indicated. For all *in vitro* assays, overnight cultures were grown in THY at 37°C with 5% CO_2 and were used to inoculate fresh, prewarmed THY for growth to culture density required. For mutant strains containing antibiotic resistance cassettes, growth media were supplemented with the corresponding antibiotic (kanamycin 150 μg/mL, chloramphenicol 10 μg/mL, kanamycin/chloramphenicol 100/10 μg/mL).

Generation of ICESpyM92 mutants. Strain backgrounds for study were chosen based on an absence of mutations in known virulence regulators. Reversion of the nonsynonymous SNP at nucleotide position 815 resulting in CovS^{S272L} mutation in the TSPY556 strain was achieved using a previously published procedure for allelic in-frame replacement of the *covS* gene (33). A counterselection approach employing a levansucrase (*sacB*) marker was adapted from Hooven et al. (34) to generate an *emm92* strain lacking the ICESpyM92 integrative-conjugative element (Δ*ICE*). ICESpyM92 was transferred into the MGAS270 strain by filter mating, as previously described by Sitkiewicz et al. (35), with modifications. Detailed protocols are included in supplemental material. Plasmids and primers used in this study are listed in Table S2.

Mouse subcutaneous infection model. GAS pathogenesis in the course of SSTI was modeled using a previously published protocol (15), with modifications, approved by the UT Health Houston Animal Welfare Committee (AWC). A bacterial suspension in saline of 2×10^8 CFU mL^{-1} (10^7 CFU infectious dose) or 2×10^7 CFU mL^{-1} (10^6 CFU infectious dose), verified by plating for viable colonies, was used to infect 3- to 4-week-old male and female CD-1 mice (Charles River Laboratories). Mice were anesthetized by isoflurane inhalation, fur was removed from an ~3cm^2 area of the haunch with Nair (Carter Products), and 50 μL of bacterial suspension was injected under the skin. Mice were monitored twice daily for 7 days and were euthanized by CO_2 asphyxiation at 48 h or day 7 postinfection, at which point infection site dermal tissue was processed for analysis. Protocol details for measurement of necrotic lesion size and infectious site GAS burden is included in supplemental material.

Mouse intraperitoneal infection model. GAS pathogenesis and invasiveness was modeled using a previously published protocol (17), with modifications, approved by the UT Health Houston AWC. A bacterial suspension in saline of 2×10^9 CFU mL^{-1} (10^8 CFU infectious dose), verified by plating for viable colonies, was used to infect 3- to 4-week-old female CD-1 mice (Charles River Laboratories). Mice were anesthetized by isoflurane inhalation, and 50 μL of bacterial suspension was injected intraperitoneally. Mice were monitored every 8 h for near-mortality over 72 h and survival was compared using Kaplan-Meier analysis. Differences in survival were calculated using a Mantel-Cox (log rank) analysis with a P value of <0.05 considered statistically significant. Protocol details for measurement of GAS burden in spleen tissue is included in supplemental material.

Exposure to primary human epidermal keratinocytes (HEK) and RNA isolation for qRT-PCR analysis. Approximately 1×10^7 CFU of GAS (multiplicity of infection of ~100) grown to midexponential phase (THY broth at an OD_{600} of 0.4) was added to 12 technical replicate wells previously seeded with human neonatal epithelial keratinocytes (HEK) cultured according to the supplier's specifications in Keratinocyte Medium (KM) (catalog number 2100, 2101; ScienCell Research Laboratories) and incubated 1 h at 37°C with 5% CO_2. HEKs were then washed (5X) with Dulbecco's Phosphate Buffered Saline to

remove nonadherent GAS. HEK with adherent GAS were then incubated in KM for an additional 2 h, at which point culture supernate was removed and adherent GAS were harvested for RNA isolation by centrifugation, following lysis of HEK upon addition of RNAShield (Zymo).

RNA sequencing and qRT-PCR analysis. Transcriptional analyses were performed according to previously described protocols (36, 37) with modifications. Protocol details are provided in supplemental material.

SUPPLEMENTAL MATERIAL

Supplemental material is available online only.

SUPPLEMENTAL FILE 1, PDF file, 3 MB.

ACKNOWLEDGMENTS

We thank James M. Musser for generously providing the MGAS270 strain.

This work was supported by funding provided by the National Institute of Allergy and Infectious Diseases (R01AI124216 and R21AI142126 to A.R.F., and T32AI141349 to L.A.V.).

The authors declare no conflicts of interest.

REFERENCES

1. Queck SY, Khan BA, Wang R, Bach T-HL, Kretschmer D, Chen L, Kreiswirth BN, Peschel A, Deleo FR, Otto M. 2009. Mobile genetic element-encoded cytolysin connects virulence to methicillin resistance in MRSA. PLoS Pathog 5:e1000533. https://doi.org/10.1371/journal.ppat.1000533.
2. Farzand R, Rajakumar K, Barer MR, Freestone PPE, Mukamolova GV, Oggioni MR, O'Hare HM. 2021. A Virulence Associated Siderophore Importer Reduces Antimicrobial Susceptibility of. Front Microbiol 12:607512. https://doi.org/10.3389/fmicb.2021.607512.
3. Anderson SE, Chin CY, Weiss DS, Rather PN. 2020. Copy number of an integron-encoded antibiotic resistance locus regulates a virulence and opacity switch in Acinetobacter baumannii AB5075. mBio 11. https://doi.org/10.1128/mBio.02338-20.
4. Barnett TC, Bowen AC, Carapetis JR. 2018. The fall and rise of Group A. Epidemiol Infect 147:e4. https://doi.org/10.1017/S0950268818002285.
5. Beres SB, Sylva GL, Barbian KD, Lei B, Hoff JS, Mammarella ND, Liu M-Y, Smoot JC, Porcella SF, Parkins LD, Campbell DS, Smith TM, McCormick JK, Leung DYM, Schlievert PM, Musser JM. 2002. Genome sequence of a serotype M3 strain of Group A Streptococcus: phage-encoded toxins, the high-virulence phenotype, and clone emergence. Proc Natl Acad Sci U S A 99:10078–10083. https://doi.org/10.1073/pnas.152298499.
6. Banks DJ, Lei B, Musser JM. 2003. Prophage induction and expression of prophage-encoded virulence factors in group A Streptococcus serotype M3 strain MGAS315. Infect Immun 71:7079–7086. https://doi.org/10.1128/IAI.71.12.7079-7086.2003.
7. Sumby P, Porcella SF, Madrigal AG, Barbian KD, Virtaneva K, Ricklefs SM, Sturdevant DE, Graham MR, Vuopio-Varkila J, Hoe NP, Musser JM. 2005. Evolutionary origin and emergence of a highly successful clone of serotype M1 group a Streptococcus involved multiple horizontal gene transfer events. J Infect Dis 192:771–782. https://doi.org/10.1086/432514.
8. Jain I, Sarkar P, Danger JL, Medicielo J, Roshika R, Calfee G, Ramalinga A, Burgess C, Sumby P. 2019. A mobile genetic element promotes the association between serotype M28 group A Streptococcus isolates and cases of puerperal sepsis. J Infect Dis 220:882–891. https://doi.org/10.1093/infdis/jiz195.
9. Roshika R, Jain I, Medicielo J, Wächter J, Danger JL, Sumby P. 2021. The RD2 pathogenicity island modifies the disease potential of the Group A. Infect Immun 89:e0072220. https://doi.org/10.1128/IAI.00722-20.
10. Fay K, Onukwube J, Chochua S, Schaffner W, Cieslak P, Lynfield R, et al. 2021. Patterns of antibiotic nonsusceptibility among invasive group A Streptococcus infections-United States, 2006–2017. Clin Infect Dis https://doi.org/10.1093/cid/ciab575.
11. Valenciano SJ, Onukwube J, Spiller MW, Thomas A, Como-Sabetti K, Schaffner W, et al. 2020. Invasive Group A Streptococcal infections among people who inject drugs and people experiencing homelessness in the United States, 2010–2017. Clin Infect Dis https://doi.org/10.1093/cid/ciaa787.
12. Sanson MA, Macias OR, Shah BJ, Hanson B, Vega LA, Alamarat Z, et al. 2019. Unexpected relationships between frequency of antimicrobial resistance, disease phenotype and Microb Genom 5. https://doi.org/10.1099/mgen.0.000316.
13. Cornick JE, Kiran AM, Vivancos R, Van Aartsen J, Clarke J, Bevan E, Alsahag M, Alaearts M, Bricio Moreno L, Jenkinson HF, Nobbs AH, Anson J, Kadioglu A, French N, Everett DB. 2017. Epidemiological and Molecular Characterization of an Invasive Group A Streptococcus. J Clin Microbiol 55:1837–1846. https://doi.org/10.1128/JCM.00191-17.
14. Musser JM, Hauser AR, Kim MH, Schlievert PM, Nelson K, Selander RK. 1991. Streptococcus pyogenes causing toxic-shock-like syndrome and other invasive diseases: clonal diversity and pyrogenic exotoxin expression. Proc Natl Acad Sci U S A 88:2668–2672. https://doi.org/10.1073/pnas.88.7.2668.
15. Vega LA, Valdes KM, Sundar GS, Belew AT, Islam E, Berge J, Curry P, Chen S, El-Sayed NM, Le Breton Y, McIver KS. 2017. The transcriptional regulator CpsY is important for innate immune evasion in Streptococcus pyogenes. Infect Immun 85. https://doi.org/10.1128/IAI.00925-16.
16. Le Breton Y, Belew AT, Freiberg JA, Sundar GS, Islam E, Lieberman J, Shirtliff ME, Tettelin H, El-Sayed NM, McIver KS. 2017. Genome-wide discovery of novel M1T1 group A streptococcal determinants important for fitness and virulence during soft-tissue infection. PLoS Pathog 13:e1006584. https://doi.org/10.1371/journal.ppat.1006584.
17. Horstmann N, Sahasrabhojane P, Suber B, Kumaraswami M, Olsen RJ, Flores A, Musser JM, Brennan RG, Shelburne SA. 2011. Distinct single amino acid replacements in the control of virulence regulator protein differentially impact streptococcal pathogenesis. PLoS Pathog 7:e1002311. https://doi.org/10.1371/journal.ppat.1002311.
18. Shea PR, Beres SB, Flores AR, Ewbank AL, Gonzalez-Lugo JH, Martagon-Rosado AJ, Martinez-Gutierrez JC, Rehman HA, Serrano-Gonzalez M, Fittipaldi N, Ayers SD, Webb P, Willey BM, Low DE, Musser JM. 2011. Distinct signatures of diversifying selection revealed by genome analysis of respiratory tract and invasive bacterial populations. Proc Natl Acad Sci U S A 108:5039–5044. https://doi.org/10.1073/pnas.1016282108.
19. Hendrickson C, Euler CW, Nguyen SV, Rahman M, McCullor KA, King CJ, Fischetti VA, McShan WM. 2015. Elimination of chromosomal island SpyCIM1 from Streptococcus pyogenes strain SF370 reverses the mutator phenotype and alters global transcription. PLoS One 10:e0145884. https://doi.org/10.1371/journal.pone.0145884.
20. Ben Zakour NL, Davies MR, You Y, Chen JHK, Forde BM, Stanton-Cook M, Yang R, Cui Y, Barnett TC, Venturini C, Ong C.-I.Y, Tse H, Dougan G, Zhang J, Yuen K-Y, Beatson SA, Walker MJ. 2015. Transfer of scarlet fever-associated elements into the group A Streptococcus M1T1 clone. Sci Rep 5:15877. https://doi.org/10.1038/srep15877.
21. Menschner L, Falke U, Konrad P, Berner R, Toepfner N. 2019. Hydrogen peroxide production of group A Streptococci (GAS) is emm-type dependent and increased at low temperatures. Curr Microbiol 76:698–705. https://doi.org/10.1007/s00284-019-01683-y.
22. Kachroo P, Eraso JM, Olsen RJ, Zhu L, Kubiak SL, Pruitt L, Yerramilli P, Cantu CC, Ojeda Saavedra M, Pensar J, Corander J, Jenkins L, Kao L, Granillo A, Porter AR, DeLeo FR, Musser JM. 2020. New pathogenesis mechanisms and

translational leads identified by multidimensional analysis of necrotizing myositis in primates. mBio 11. https://doi.org/10.1128/mBio.03363-19.
23. Watson ME, Nielsen HV, Hultgren SJ, Caparon MG. 2013. Murine vaginal colonization model for investigating asymptomatic mucosal carriage of Streptococcus pyogenes. Infect Immun 81:1606–1617. https://doi.org/10.1128/IAI.00021-13.
24. Zhu L, Olsen RJ, Beres SB, Eraso JM, Saavedra MO, Kubiak SL, Cantu CC, Jenkins L, Charbonneau ARL, Waller AS, Musser JM. 2019. Gene fitness landscape of group A streptococcus during necrotizing myositis. J Clin Invest 129:887–901. https://doi.org/10.1172/JCI124994.
25. Hirose Y, Yamaguchi M, Okuzaki D, Motooka D, Hamamoto H, Hanada T, Sumitomo T, Nakata M, Kawabata S. 2019. Streptococcus pyogenes transcriptome changes in the inflammatory environment of necrotizing fasciitis. Appl Environ Microbiol 85. https://doi.org/10.1128/AEM.01428-19.
26. Hirose Y, Yamaguchi M, Sumitomo T, Nakata M, Hanada T, Okuzaki D, Motooka D, Mori Y, Kawasaki H, Coady A, Uchiyama S, Hiraoka M, Zurich RH, Amagai M, Nizet V, Kawabata S. 2021. Streptococcus pyogenes upregulates arginine catabolism to exert its pathogenesis on the skin surface. Cell Rep 34:108924. https://doi.org/10.1016/j.celrep.2021.108924.
27. Cusumano ZT, Watson ME, Caparon MG. 2014. Streptococcus pyogenes arginine and citrulline catabolism promotes infection and modulates innate immunity. Infect Immun 82:233–242. https://doi.org/10.1128/IAI.00916-13.
28. Siemens N, Snäll J, Svensson M, Norrby-Teglund A. 2020. Pathogenic mechanisms of Streptococcal necrotizing soft tissue infections. Adv Exp Med Biol 1294:127–150. https://doi.org/10.1007/978-3-030-57616-5_9.
29. Escudeiro P, Pothier J, Dionisio F, Nogueira T. 2019. Antibiotic resistance gene diversity and virulence gene diversity are correlated in human gut and environmental microbiomes. mSphere 4. https://doi.org/10.1128/mSphere.00135-19.
30. Qin L, McCausland JW, Cheung GY, Otto M. 2016. PSM-Mec-A virulence determinant that connects transcriptional regulation, virulence, and antibiotic resistance in Staphylococci. Front Microbiol 7:1293. https://doi.org/10.3389/fmicb.2016.01293.
31. Billard-Pomares T, Clermont O, Castellanos M, Magdoud F, Royer G, Condamine B, Fouteau S, Barbe V, Roche D, Cruveiller S, Médigue C, Pognard D, Glodt J, Dion S, Rigal O, Picard B, Denamur E, Branger C. 2019. The arginine deiminase operon is responsible for a fitness trade-off in extended-spectrum-β-lactamase-producing strains of Escherichia coli. Antimicrob Agents Chemother 63. https://doi.org/10.1128/AAC.00635-19.
32. Active Bacterial Core Surveillance Report, Emerging Infections Program Network, Group A Streptococcus. 2019. Centers for Disease Control and Prevention, 2019.
33. Flores AR, Jewell BE, Olsen RJ, Shelburne SA, Fittipaldi N, Beres SB, Musser JM. 2014. Asymptomatic carriage of group A streptococcus is associated with elimination of capsule production. Infect Immun 82:3958–3967. https://doi.org/10.1128/IAI.01788-14.
34. Hooven TA, Bonakdar M, Chamby AB, Ratner AJ. 2019. A counterselectable sucrose sensitivity marker permits efficient and flexible mutagenesis in Streptococcus agalactiae. Appl Environ Microbiol 85. https://doi.org/10.1128/AEM.03009-18.
35. Sitkiewicz I, Green NM, Guo N, Mereghetti L, Musser JM. 2011. Lateral gene transfer of streptococcal ICE element RD2 (region of difference 2) encoding secreted proteins. BMC Microbiol 11:65. https://doi.org/10.1186/1471-2180-11-65.
36. Sanson MA, Vega LA, Shah B, Regmi S, Cubria MB, Horstmann N, Shelburne SA, Flores AR. 2021. The LiaFSR transcriptome reveals an interconnected regulatory network in group A. Infect Immun 89:IAI0021521. https://doi.org/10.1128/IAI.00215-21.
37. Sanson M, Flores AR. 2020. Group A Streptococcus transcriptome analysis. Methods Mol Biol 2136:113–133. https://doi.org/10.1007/978-1-0716-0467-0_8.